



Selective vapor-phase hydrodeoxygenation of anisole to benzene on molybdenum carbide catalysts



Wen-Sheng Lee, Zhenshu Wang, Ryan J. Wu, Aditya Bhan*

Department of Chemical Engineering and Materials Science, University of Minnesota, Minneapolis, MN 55455, United States

ARTICLE INFO

Article history:

Received 17 April 2014

Revised 30 July 2014

Accepted 31 July 2014

Keywords:

Lignin upgrading

Anisole

Benzene

Molybdenum carbide

Hydrodeoxygenation

ABSTRACT

Vapor-phase hydrodeoxygenation (HDO) of anisole over Mo₂C catalysts at low temperatures (420–520 K) and ambient pressure showed (1) remarkable selectivity for C–O bond cleavage, giving benzene selectivity >90% among C₆ products, (2) high hydrogen efficiency for the HDO reaction as indicated by low cyclohexane selectivity (<9%), and (3) good stability over ~50 h. Methane selectivity increased at the expense of methanol selectivity as anisole conversion increased, suggesting that the phenolic C–O bond was cleaved preferentially. The concurrent near half-/zero-order dependence of benzene synthesis rates on H₂/anisole pressure, and the preferential inhibition of benzene synthesis rates upon introduction of CO relative to isotopic HD exchange suggest that catalytic sites for H₂ activation are distinct from those required for the activation of anisole. The involvement of metallic sites on Mo₂C catalysts for this reaction was demonstrated by the nearly invariant benzene synthesis rate per CO chemisorption site.

© 2014 Elsevier Inc. All rights reserved.

1. Introduction

Utilization of biogenic sources as an alternative carbon feedstock to produce fuels and chemicals has drawn a lot of attention because of sustainability and environmental concerns [1–3]. In this context, the lignin fraction of lignocellulosic biomass represents the most viable source to produce aromatic compounds. Hydrodeoxygenation (HDO) of phenolic ethers derived from lignin results in the synthesis of aromatic compounds such as benzene, toluene, and xylene (BTX) [4–7]. High selectivity to cleavage of the phenolic C–O bond, which gives aromatics products, is desired, but concurrently challenging because of its strong bond strength (422–468 kJ mole⁻¹) [1]. Severe reaction conditions with both high reaction temperature (500–700 K), which facilitates phenolic C–O bond cleavage [1,8–10] and high hydrogen pressure (1–30 MPa), which alleviates catalyst deactivation by reducing coke formation [8,11–13] are typically used for HDO of phenolic compounds to give aromatic products. This accompanies potential issues such as (i) excess hydrogen consumption and/or loss of aromaticity via unwanted hydrogenation and/or (ii) reduction of the carbon chain length via hydrogenolysis reactions, and/or (iii) low selectivity to desired deoxygenated aromatics due to other side reactions such as alkylation/transalkylation promoted by high reaction temperatures [14,15].

Anisole has been widely chosen as a model compound for lignin-derived phenolics because it contains a methoxyl group (–OCH₃), one of the major oxygen-containing functional groups found in lignin-derived compounds [12,15–21]. Low selectivity (<25%) to the desired deoxygenated aromatics (i.e., benzene) but high selectivity (>40%) to phenol was found for anisole HDO with conventional hydrotreating Co–Mo sulfide catalysts (either in the liquid or in the vapor phase) at different conditions with temperatures ranging from 523 to 560 K and total pressures ranging from 1.5 to 50 MPa [18,22,23], suggesting that Co–Mo-based catalysts preferentially break the weaker aliphatic C–O bond (~339 kJ mole⁻¹), not the phenolic C–O bond, in anisole. Transition metal phosphides, a potential new class of hydroprocessing catalysts [24–26], have also been investigated (Ni₂P/SiO₂, MoP/SiO₂ and NiMoP/SiO₂) for anisole HDO in a fixed bed reactor [17]. While the selectivity to deoxygenated products (benzene and cyclohexane) can reach almost ~100% at 573 K and 1.5 MPa, the benzene selectivity was found to be less than 20%, suggesting inefficient usage of H₂ for the HDO reaction. Similarly, benzene selectivity was found to be only ~30–46% at 498–548 K under 50 atm H₂ when using copper chromite as a catalyst for liquid-phase anisole HDO [16]. Vapor-phase anisole HDO over noble metal catalysts such as Pt/Al₂O₃ at 573 K and near ambient pressure (~140 kPa) resulted in benzene selectivity as low as ~4.4% and high phenol selectivity (~65%) [21]. Pt–Sn bimetallic catalysts showed higher benzene yield than either Pt or Sn monometallic catalysts for vapor-phase guaiacol HDO reactions; however, these bimetallic

* Corresponding author. Fax: +1 612 626 7246.

E-mail address: abhan@umn.edu (A. Bhan).

formulations still resulted in aromatic yields less than 50% for vapor-phase anisole HDO reactions at 673 K and atmospheric pressure [12].

High selectivity to deoxygenation products with selectivity to benzene ~50%, toluene ~25%, and xylene ~10% at ~673 K under 1 atm, however, was reported when an acidic function (H-BEA) was introduced together with a metal function (Pt) [15]. Hicks and coworkers recently reported that high selectivity to benzene among C_6 products (~90%) for anisole HDO reactions in the liquid phase with toluene as a solvent could be obtained using bimetallic FeMo phosphide (FeMoP) catalysts; however, high hydrogen pressures ~2.1 MPa and high reaction temperatures ~673 K were required to accomplish this selective deoxygenation [19]. MoO_3 , which showed the highest specific rates for acetone HDO among other reducible metal oxides such as V_2O_5 , Fe_2O_3 , CuO , and WO_3 via a reverse Mars-van Krevelen mechanism, was also tested for vapor-phase anisole HDO at 673 K under ambient pressure [27]. A mixture of deoxygenated aromatics was observed in which the selectivity of benzene, toluene, xylene, and alkylbenzenes was ~60%, ~20%, ~6.5%, and ~13%, respectively [27]. No observation of sequential hydrogenation products of the aforementioned aromatics was reported, implying that this process is hydrogen efficient [27].

Recently, transition metal carbides have been reported to selectively remove oxygen from C_2 – C_3 oxygenates [28,29], vegetable oils [30], stearic acid [4], and guaiacol [31]. Herein, we report that Mo_2C is a selective HDO catalyst for phenyl ethers at low temperatures (~420–520 K) under atmospheric pressure with good catalyst stability over the course of ~50 h, in which benzene can be formed almost exclusively with >90% selectivity among C_6 products. The high hydrogen efficiency of this process is evidenced by the low selectivity (<9%) to cyclohexane in successive hydrogenation reactions of benzene even at high hydrogen-to-oxygenate molar ratios (~700) in the reactant feed. Plausible reaction mechanisms in which two distinct catalytic sites are involved for vapor-phase anisole HDO on Mo_2C catalysts are proposed based on detailed kinetic measurements performed in this work. Metallic sites on Mo_2C catalysts are involved in the reaction as inferred from the near invariance in benzene synthesis rates normalized by the number of catalytic centers measured by *ex situ* CO chemisorption, although the requirement of carbidic or oxycarbidic sites for HDO chemistry remains ambiguous at this point.

2. Experimental methods

2.1. Catalyst synthesis

Mo_2C catalysts were prepared based on a prior report with ammonium molybdate tetrahydrate ($(NH_4)_6Mo_7O_{24} \cdot 4H_2O$) as a precursor [28,32]. Mo_2C catalysts with varying number of CO adsorption sites were obtained using varying temperature and flow rate protocols that are described in detail below. An appropriate amount (0.6–6 g) of ammonium molybdate tetrahydrate (sieved, 177–400 μm , Sigma, 99.98%, trace metal basis; typically ~0.6 g) was loaded in a tubular quartz reactor (I.D. 10 mm) and purged with a desired total flow rate (1.09–2.93 $cm^3 s^{-1}$; typically 2.93 $cm^3 s^{-1}$), consisting of either 15/85 vol% of CH_4 (Matheson, 99.97%) and H_2 (Minneapolis Oxygen, 99.999%) mixture or pure H_2 at room temperature (RT) for about 1–5 min (typically in CH_4/H_2 mixture). The reactor was then heated in a three-zone split tube furnace (Series 3210, Applied Test System) from RT to the first target temperature (~618–623 K, typically 623 K) within 1.5 h, and the temperature was then held for 12–24 h. Subsequently, the sample was heated in a CH_4/H_2 (15/85 vol%) gas mixture (the gas mixture either remained unchanged or CH_4 was added to the

existing pure H_2 flow to give the desired composition) to the final target temperature (~863–978 K, typically 863 K) within 1.5 h and held at the final temperature for 2–6 h (typically 2 h) and then cooled down to RT in the CH_4/H_2 (15/85 vol%) gas mixture flow. The resulting material was then treated in a flowing 1% O_2/He mixture (Matheson, Certified Standard Purity) at ~1.67–3.33 $cm^3 s^{-1}$ for at least 2 h before being removed from the reactor to passivate the carbidic surface [33]. Thus, a typical protocol for the Mo_2C catalyst preparation (sample#8 in Table 1), “ CH_4/H_2 -RT(1.5 h)-623 K[12 h](1.5 h)-863 K[2 h]-cool”, represents that the ammonium molybdate tetrahydrate in the reactor was exposed to a gas environment of CH_4/H_2 mixture and heated up to 623 K within 1.5 h and held at 623 K for 12 h. After that, the temperature was increased to 863 K within 1.5 h. Finally, the reactor was held at 863 K for 2 h and then cooled down to RT. Even though the preparation conditions were carefully controlled in this work, different batches of Mo_2C catalysts may have small variations in their physical/chemical properties because the degree of carburization as well as the amount of carbon deposition was found to be sensitive to the carburization conditions [34,35]. Therefore, samples #1–8 listed in Table 1 consisted of multiple batches of Mo_2C synthesized with the corresponding preparation conditions to create a representative Mo_2C catalyst that shares a set of physical/chemical properties. Sample #9 in Table 1, however, was prepared by re-carburizing a mixture of multiple batches of Mo_2C with different amounts of CO chemisorption sites at 323 K (~6 g) in a CH_4/H_2 mixture (14/86 vol%, ~9.66 $cm^3 s^{-1}$) using a temperature protocol shown in Table 1. We note that the fresh, passivated sample was stored in a vial (ambient conditions) and exposed to air before the kinetic measurements and aged <1 month prior to the characterization discussed below.

Pd/Al_2O_3 (~1 wt% Pd) catalysts were prepared by an incipient wetness method in which ~1 g of alumina (Sasol North America Inc., pretreated in a flow of dry air (ultrapure, Minneapolis Oxygen) with a total flow rate ~1.67 $cm^3 s^{-1}$ at 723 K (0.012 $K s^{-1}$) for 4 h prior to usage) was impregnated with an appropriate amount of Pd solution ($Pd(NO_3)_2 \cdot 2H_2O$, ~40% metal basis, Sigma Aldrich). After impregnation, samples were dried in a static oven at ~363 K overnight, followed by treatment in a flow of dry air (~1.67 $cm^3 s^{-1}$) at 363 K (0.012 $K s^{-1}$) for 9 h and subsequently heated at 823 K (0.025 $K s^{-1}$) for 4 h.

2.2. Materials characterization

Unless otherwise mentioned, a representative fresh, passivated Mo_2C sample, sample#8 in Table 1, was used for the characterization protocol discussed below. The bulk structures of both spent and fresh samples were determined using X-ray diffraction (XRD, Bruker D8 Discover 2D X-ray diffractometer with a two-dimensional VANTEC-500 detector, $Cu K_{\alpha}$ X-ray radiation with a graphite monochromator, and a 0.5 mm point collimator). The sample was drop casted on a SiO_2 zero-background holder and measured in three measurement frames at 30° (2θ), 60° (2θ) and 90° (2θ) with a 600 s frame⁻¹ dwell ($\Delta\theta$ frame width of 35° (2θ)). Two-dimensional images were then converted to one-dimensional intensity vs. 2θ for analysis. The crystallite size of the sample was estimated using the Scherrer equation [35]. The particle morphologies of the sample were characterized via transmission electron microscopy (TEM FEI Tecnai T12, 120 keV). For TEM sample preparation, the Mo_2C catalyst was sonicated in dimethylformamide (DMF, Sigma, 99.8% ACS reagent) for 2 h and a drop was placed onto a holey-carbon Cu grid and then dried at 353 K in a vacuum oven overnight prior to the TEM analysis. The BET surface area (S_g), pore volume, and mesopore size distribution (obtained by Barrett–Joyner–Halenda (BJH) analysis at desorption branch) were measured using N_2 adsorption/desorption isotherms (Micromeritics

Table 1
Preparation conditions for high surface area Mo₂C samples with varying numbers of catalytic centers measured by CO chemisorption at 323 K.

| Catalysts | AMT ^a (g) | CH ₄ flow rate (cm ³ s ⁻¹) | H ₂ flow rate (cm ³ s ⁻¹) | Temp profile ^c | CO uptake at 323 K (μmole g ⁻¹ , STP) ^d |
|-----------|----------------------|--|---|---|---|
| #1 | 3.0 | 0.44 | 0.65 | CH ₄ /H ₂ -RT(1.5 h)-623 K[24 h](1.5 h)-873 K[6 h]-cool | 51 |
| #2 | 6.0 | 0.44 | 2.49 | CH ₄ /H ₂ -RT(1.5 h)-623 K[12 h](1.5 h)-978 K[3 h]-cool | 92 |
| #3 | 2.4 | 0.44 | 2.49 | H ₂ -RT(1.5 h)-618 K[15 h]-CH ₄ /H ₂ (1.5 h)-863 K[2 h]-cool | 101 |
| #4 | 6.0 | 0.44 | 2.49 | H ₂ -RT(1.5 h)-618 K[15 h]-CH ₄ /H ₂ (1.5 h)-863 K[2 h]-cool | 120 |
| #5 | 0.6 | 0.44 | 2.49 | CH ₄ /H ₂ -RT(1.5 h)-623 K[12 h](1.5 h)-873 K[2 h]-cool | 122 |
| #6 | 3.6 | 0.44 | 2.49 | CH ₄ /H ₂ -RT(1.5 h)-623 K[12 h](1.5 h)-858 K[4 h]-cool | 130 |
| #7 | 0.6 | 0.29 | 1.66 | H ₂ -RT(1.5 h)-618 K[15 h]-CH ₄ /H ₂ (1.5 h)-863 K[2 h]-cool | 163 |
| #8 | 0.6 | 0.44 | 2.49 | CH ₄ /H ₂ -RT(1.5 h)-623 K[12 h](1.5 h)-863 K[2 h]-cool | 220 |
| #9 | 6.0 ^b | 1.33 | 8.33 | CH ₄ /H ₂ -RT(1.5 h)-623 K[0 h](1.5 h)-908 K[3 h]-cool | 152 |
| #10 | 1.5 | 0.42 | 2.33 | CH ₄ /H ₂ -RT(1.5 h)-628 K[5 h](1.5 h)-883 K[3 h]-cool | 208 |

^a Ammonium molybdate tetrahydrate ((NH₄)₆Mo₇O₂₄·4H₂O, sieved 177–400 μm).

^b Samples were prepared by re-carburizing a mixture of multiple batches of Mo₂C catalysts (~6 g) with different amounts of CO chemisorption sites using the conditions shown in this table.

^c Detailed description for the preparation conditions can be found in Section 2.1. For the catalysts prepared from heating in the pure H₂ environments first, such as sample #3 (H₂-RT(1.5 h)-618 K[15 h]-CH₄/H₂(1.5 h)-863 K[2 h]-cool), the switch of H₂ to CH₄/H₂ was achieved by adding CH₄ (0.44 cm³ s⁻¹) to the existing H₂ flow (2.49 cm³ s⁻¹).

^d Except for sample #8 and #10 in which CO chemisorption were measured within one day of the Mo₂C catalyst synthesis, the rest of the samples were stored in vials for a few weeks prior to both CO chemisorption and the kinetic measurements. The CO chemisorption and the kinetic measurements were, however, carried out on the same day for each sample listed above.

ASAP 2020). The sample was degassed (<6 μmHg) at 523 K for at least 4 h before N₂ adsorption. CO (Matheson, 99.5%) chemisorption uptakes were measured at 323 K using a Micromeritics ASAP 2020 instrument. CO chemisorption measurements for all samples shown in Table 1 were carried out following the procedure described below. The cell loaded with the Mo₂C catalyst (0.05–0.2 g) was first evacuated at 383 K (~2 μmHg) for 0.5 h, and then treated in H₂ at 723 K for 2 h, followed by degassing (~2 μmHg) at 723 K for 2 h. The sample was subsequently cooled to 323 K prior to the first adsorption isotherm measurement (between 100 and 450 mmHg). The cell was then degassed (~2 μmHg) to remove weakly adsorbed species prior to the second isotherm. Both isotherms were

were heated to at least 373 K via resistive heating to prevent condensation of effluents sent to a mass spectrometer (MKS Cirrus 200 Quadrupole MS system) and a gas chromatograph (Agilent 6890) equipped with a methyl-siloxane capillary column (HP-1, 50 m × 320 μm × 0.52 μm) connected to a flame ionization detector (FID). The concentration of analytes from reactor effluents was quantified with an external standard method in which the corresponding GC calibration curves with R² values >0.96 and at least 4 different concentrations ensured precise measurement of the concentration of products of interest. The carbon balance was typically better than 92%. The anisole conversion and product selectivity are calculated as follows:

Anisole conversion = (sum of the carbon in products)/moles of carbon in anisole);

C₆⁺ product selectivity = (moles of C₆⁺ product i)/(∑ moles of C₆⁺ products).

C₁ products selectivity = (mole of methane or methanol)/(mole of methane + mole of methanol)

extrapolated to zero pressure to determine the total (from the first isotherm) and weakly adsorbed (from the second isotherm) species. The amount of irreversibly or strongly adsorbed species was obtained by the difference between two extrapolated values [35,36]. The procedure for H₂ chemisorption of 1 wt% Pd/Al₂O₃ catalysts used for H₂-D₂-CO titration experiments (Section 3.3) is similar to that for the CO chemisorption of Mo₂C catalysts except the Pd sample was pretreated in H₂ at 523 K for 1 h prior to H₂ chemisorption at 323 K and irreversibly adsorbed H₂ was used to calculate the Pd metal dispersion by assuming a hydrogen-to-metal stoichiometry of one.

2.3. Kinetic measurements of vapor-phase anisole HDO on Mo₂C catalysts

Vapor-phase anisole hydrodeoxygenation (HDO) rates were measured using a tubular quartz reactor (I.D. 10 mm) with an outer thermowell at the bottom of the reactor for holding a thermocouple to monitor reaction temperature. Catalysts (0.03–0.14 g) were treated in pure H₂ (~1.67 cm³ s⁻¹) at ~750 K for 1 h and cooled down to a typical reaction temperature ~423 K before introducing the reaction mixture (~1.67 cm³ s⁻¹) consisting of ~0.14/bal (vol%) of anisole and H₂. Anisole (Sigma, 99%, ReagentPlus) was added using a syringe pump (KD Scientific, Model 100). All flow lines

Kinetic studies were conducted in a differential reactor bed in which anisole conversion was controlled to be <15%. The absence of heat and external mass transfer limitations was confirmed by estimating Mears' criteria (Table S1, SI). The benzene turnover rate was independent of linear velocities of the reactants (Fig. S1, SI), demonstrating that the reaction rate was not limited by external mass transfer. Internal mass transfer limitations can be neglected because the estimated Thiele modulus was significantly less than 1 (Table S2, SI).

H₂-D₂ exchange reactions were performed by flowing a gas mixture (~1.67 cm³ s⁻¹) consisting of anisole/D₂/H₂/Ar (vol%) = ~0.12/40/40/bal to a reactor packed with a mixture of ~0.022 g of Mo₂C catalysts (sample #10 in Table 1) and ~0.45 g quartz sand (washed with 1 M HNO₃ solution and treated in a flow of air at 1073 K for 2 h prior to usage), which had been tested under standard reaction conditions (STD, reaction mixture consisting of anisole/H₂ (vol%) = 0.12/bal with total flow rate ~1.67 cm³ s⁻¹ at 406 K) for ~2 h. The net rates of H/D exchange were measured by using online mass spectrometry (MS, MKS Cirrus 200 Quadrupole MS system). The mass spectrometer was calibrated by flowing a gas mixture with varying H₂/D₂ compositions through a reactor packed with a mixture of ~0.2 g Pd/Al₂O₃ catalysts (Pd loading ~1 wt%, and metal dispersion ~12% by H₂ chemisorption measured at 323 K) and ~1 g quartz sand at ~463 K to obtain the

corresponding equilibrated H₂/D₂ mixture. The Pd catalysts were activated by flowing H₂ ($\sim 1.67 \text{ cm}^3 \text{ s}^{-1}$) at 573 K for 1 h with a ramping rate $\sim 0.05 \text{ K s}^{-1}$ from RT before calibrating the mass spectrometer for HD. The error associated with HD quantification by online mass spectrometry, calculated from 11 independent measurements of the HD response factor, was found to be <10%. The measured reversibility of H/D exchange, η_{HD} , was estimated to be ~ 0.1 . Rates of H/D exchange are reported as forward rates of H/D exchange, which were obtained by dividing the net rate of H/D exchange by $(1 - \eta_{\text{HD}})$.

3. Results and discussion

3.1. Characterization of Mo₂C

The absence of peaks assigned to the MoO₃ crystalline phase, as shown in Fig. 1, suggests that bulk carburization was achieved. β -Mo₂C (Joint Committee on Powder Diffraction Standards, No. 35-0787, 2θ peaks at $\sim 34.355^\circ$ (100), 37.979° (002), 39.393° (101), 52.124° (102), 61.529° (110), 69.567° (103), 74.647° (112), and 75.514° (201)) was identified as the major carbidic phase and α -MoC_{1-x} as the minor phase based on the comparison of the observed XRD peak intensities from both phases. The materials are, therefore, referred to as Mo₂C formulations because the Mo/C molar ratio is near two in both phases. An impurity phase that contributed the signal at $\sim 26^\circ$ (2θ), was also found in the fresh, passivated Mo₂C catalyst (Fig. 1). Both MoO₂ and Mo(CO)₆ might be the source of the impurity based on the comparison between the observed XRD pattern and the references of MoO₂ (JCPDS No. 32-0671) and Mo(CO)₆ (JCPDS No. 12-0691) (see Fig. S2(a) in the SI). Although our XRD analysis does not allow us to distinguish between Mo(CO)₆ and MoO₂, the impurity could be residual MoO₂ with poor crystallinity since the formation of MoO₂ was observed during the carburization process with ammonium molybdate as the Mo₂C precursor by Djéga-Mariadassou and coworkers [34]. The observation of two different phases, β -Mo₂C and α -MoC_{1-x}, and the impurity phase at $\sim 26^\circ$ (2θ) for the Mo₂C catalyst synthesized in this work is consistent with those reported by Thompson and coworkers [32]. The peak at $\sim 26^\circ$ (2θ), however, was not observed for Mo₂C catalysts prepared by re-carburization (sample #9 in Table 1, passivated prior to XRD measurement) in a CH₄/H₂ mixture flow (14/86 vol%, $\sim 9.66 \text{ cm}^3 \text{ s}^{-1}$) as shown in Fig. S2(b) in the SI. The presence of this impurity phase, however, was found to have a negligible effect on the catalytic performance in vapor-phase anisole HDO, as inferred from similar benzene

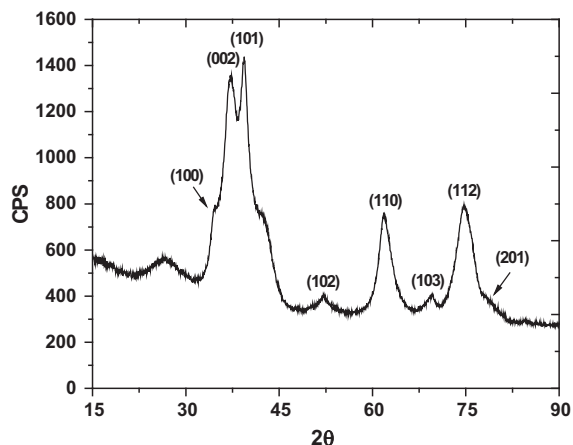


Fig. 1. X-ray diffraction pattern for the fresh, passivated Mo₂C catalyst (sample #8 in Table 1).

synthesis rates for sample #8 and #9 ($\sim 3 \times 10^{-4} \text{ mole s}^{-1} \text{ mole}^{-1} \text{ c}_{\text{Osite}}$, Table 2), which will be discussed in Section 3.3.

The crystallite size of β -Mo₂C for the fresh, passivated Mo₂C catalyst (sample #8 in Table 1), estimated using the Scherrer equation for the 2θ peak at $\sim 52^\circ$ (the peak intensity has contributions only from β -Mo₂C phase), was found to be $\sim 3.3 \text{ nm}$, which is comparable to that reported by Boudart and coworkers for Mo₂C catalysts ($\sim 5.8 \text{ nm}$) prepared using MoO₃ as the precursor [35]. The BET surface area and the amount of irreversibly chemisorbed CO at $\sim 323 \text{ K}$ for a typical fresh, passivated Mo₂C catalyst (sample #8 in Table 1) were $\sim 116 \text{ m}^2 \text{ g}^{-1}$ and $220 \mu\text{mole g}^{-1}$ (STP) respectively, which is in good agreement with results reported by Thompson and coworkers [32]. Porous features of a typical fresh, passivated Mo₂C catalysts were evidenced by the following: (1) the existence of a hysteresis loop observed in the relative pressure (P/P^0) range of 0.4–0.8, characteristic of multilayer adsorption occurring inside mesopores in the N₂ adsorption isotherms, as shown in Fig. 2; (2) the observed contrast regions inside a representative Mo₂C particle from TEM analysis, as shown in Fig. 3. Furthermore, the theoretical (100) interplanar distance matched the spacing of the lattice fringes, confirming the presence of the β -Mo₂C structure. The average mesopore diameter and pore volume (at $P/P^0 \sim 0.99$) were found to be $\sim 6.4 \text{ nm}$ (BJH desorption branch) and $0.14 \text{ cm}^3 \text{ g}^{-1}$ respectively. A typical fresh, passivated Mo₂C catalyst was in polycrystalline form as evidenced by the arrangement of discrete spots observed in the selected area electron diffraction (SAED) of a typical Mo₂C particle (not shown) consistent with the results reported by Bell and coworkers [37]. The much larger particle size ($D_p \sim 70 \text{ nm}$, estimated by BET surface area (S_g) using the equation $D_p \sim 6 (\rho \times S_g)^{-1}$ where ρ is the bulk density of the Mo₂C catalyst, reported to be around $\sim 760 \text{ kg m}^{-3}$ [38]), as compared to the crystallite size ($\sim 3.3 \text{ nm}$) determined by XRD, also suggests the synthesized Mo₂C catalyst is polycrystalline.

3.2. Kinetics of vapor-phase anisole HDO on Mo₂C catalysts

Fig. 4 shows the conversion and selectivity for vapor-phase anisole HDO on a Mo₂C catalyst (sample #8 in Table 1) over a temperature range of 420–520 K at ambient pressure. The time-on-stream behavior of the catalyst showed that <20% deactivation occurred after two temperature cycles (420 K–520 K–472 K) over a time period of $\sim 50 \text{ h}$, implying Mo₂C catalysts are significantly more stable than Pt- or Co–Mo-based catalysts, which typically showed >20% deactivation within $\sim 5 \text{ h}$ [12,15,18]. The selectivities of all major products (benzene, cyclohexane (Fig. 4(b)), methane, and methanol (Fig. 4(c))) at a given temperature (e.g., 472 K) during the second temperature cycle, were found to be the same as those measured during the first temperature cycle, indicating that catalyst deactivation was caused by a change in the number and not the chemistry or identity of the active sites.

There are two possible reasons for catalyst deactivation: (i) carbon deposition, which can directly block the active sites and/or occlude catalyst mesopores resulting in the loss of the surface area (and hence the active sites) [15,16,18], and (ii) slow oxidation of the Mo₂C catalyst to form an oxycarbide and/or oxide phases at the surface or the sub-surface upon exposure to the oxygen-containing reactant. A cause of catalyst deactivation is the formation of carbonaceous species occurred during high temperature cycles because no sign of catalyst deactivation was found for another independent catalyst stability test at 420 K for more than 15 h. (Fig. S3(a), SI); however, oxidation of the carbidic surface at higher reaction temperatures cannot be excluded. Our research does not distinguish between these deactivation mechanisms and instead focuses on understanding the kinetics, mechanism, and site requirements of vapor-phase anisole HDO.

Table 2
Catalytic performance (benzene turnover rate (TOR), benzene selectivity and apparent Ea) of vapor-phase anisole HDO for high surface area Mo₂C samples with varying numbers of catalytic centers measured by CO chemisorption at 323 K.

| Catalysts ^a | CO uptake at 323 K ($\mu\text{mole g}^{-1}$, STP) ^b | Benzene TOR at 423 K ($\times 10^{-4}$ mole s ⁻¹ mole _{COsite} ⁻¹) ^c | Benzene selectivity (%) ^c | Apparent activation energy, Ea (kJ mole ⁻¹) |
|------------------------|---|---|---|--|
| #1 | 51 | 4.2 | 93 | 75.8 \pm 1.8 |
| #2 | 92 | 3.1 | 91 | 72.7 \pm 0.8 |
| #3 | 101 | 2.7 | 91 | 71.5 \pm 1.3 |
| #4 | 120 | 2.9 | 91 | 69.3 \pm 4.5 |
| #5 | 122 | 3.0 | 90 | 71.0 \pm 0.4 |
| #6 | 130 | 4.3 | 94 | 67.8 \pm 1.8 |
| #7 | 163 | 5.7 | 94 | 69.3 \pm 1.8 |
| #8 | 220 | 3.0 ^d | 92 | ND |
| #9 | 152 | 2.7 ^d | 91 | ND |
| #10 | 208 | 2.6 ^e | 92 | ND |

ND: not determined.

^a Detailed preparation conditions for the listed samples can be found in Table 1.

^b Except for sample #8 and #10 in which CO chemisorption were measured within one day of the Mo₂C catalyst synthesis, the rest of the samples were stored in vials for a few weeks prior to both CO chemisorption and the kinetic measurements. The CO chemisorption and the kinetic measurements were carried out on the same day for each sample listed above.

^c The reported rate represents an average value at 423 K between 1–2 h time-on-stream with anisole conversion <14%. Reaction conditions: anisole/H₂ = ~0.14%/bal (1.67 cm³ s⁻¹) at ~423 K; catalyst loading: 80–250 mg.

^d Reaction temperature was ~420 K. Apparent activation energy ~70 kJ mole⁻¹ was used to calculate the rate at 423 K by extrapolation.

^e The reported rate represents an average value between 1–2 h time-on-stream with reaction conditions: anisole/H₂ = ~0.14%/bal (1.67 cm³ s⁻¹) at 406 K prior to H₂-D₂-CO titration experiment shown in Fig. 9 with catalyst loading: ~0.022 g. Apparent activation energy ~70 kJ mole⁻¹ was used to calculate the rate at 423 K by extrapolation.

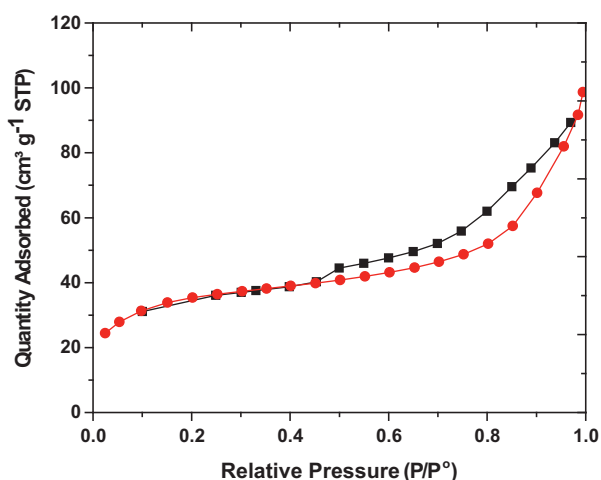


Fig. 2. N₂ adsorption (●)/desorption (■) isotherm at 77 K for the fresh, passivated Mo₂C catalyst (sample #8 in Table 1).

An independent kinetic study was conducted to assess the structural evolution of Mo₂C formulations during anisole HDO. Steady-state rates of anisole HDO were measured on a Mo₂C catalyst (sample #9 in Table 1) at ~420 K and ambient pressure (Fig. S3(b), SI). The catalyst was then cooled down to RT in flowing He (~3.33 cm³ s⁻¹); subsequently treated in a flowing 1% O₂/He mixture (~3–4 cm³ s⁻¹) for 1 h prior to XRD analysis. The catalyst bed temperature increased from RT to ~333 K upon exposure to the 1% O₂/He mixture suggesting that the catalyst, after exposure to the reactant mixture, was still pyrophoric in nature. No noticeable change was observed in the XRD pattern for the spent Mo₂C catalysts (Fig. S2(b), SI), suggesting the bulk structure of the catalyst remained in carbidic form after the HDO reaction.

Benzene selectivity was found to be >90% based on C₆⁺ products over anisole chemical conversions ranging from 10% to 100% for the Mo₂C formulations we report, which contrasts with the low selectivity (<50%) to deoxygenated aromatics (i.e., benzene) obtained using commercial hydrotreating (Co–Mo-based [18,22,23], Pt-based [12,15,21], transition metal phosphide (Ni₂P, MoP, and NiMoP) [17], or copper chromite [16] catalysts at high hydrogen pressures (1–5 MPa) and high temperatures

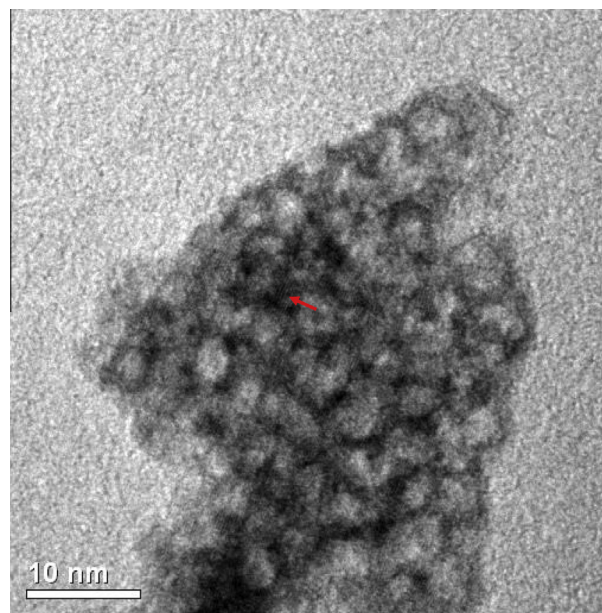


Fig. 3. A representative TEM image of the fresh, passivated Mo₂C catalyst (sample #8 in Table 1). Lattice fringes (indicated by arrow) corresponding to the (100) plane of β -Mo₂C were identified.

(523–673 K), but is comparable to the performance of bimetallic FeMo phosphides (FeMoP) catalysts for liquid-phase anisole HDO reaction reported by Hicks and coworkers [19]. While the overall selectivity to deoxygenated products for vapor-phase anisole HDO reaction was found to be similar (>90%) between the Mo₂C catalysts reported here and the MoO₃ catalysts reported by Roman-Leshkov and coworkers [27], negligible transalkylation activity was observed for the Mo₂C catalysts with the sum of the selectivity to toluene and styrene being less than 2% at all anisole conversions.

No C₂–C₅ products were observed at all reaction temperatures, suggesting that Mo₂C catalysts are very selective in cleaving C–O bonds instead of C–C bonds. The ratio of the sum of C₁ synthesis rates (methanol + methane, denoted as C₁ rates) to the sum of C₆ synthesis rates (benzene + cyclohexane, denoted as C₆ rates) for the data shown in Fig. 4 was found to be near 1 (Fig. S5 in the

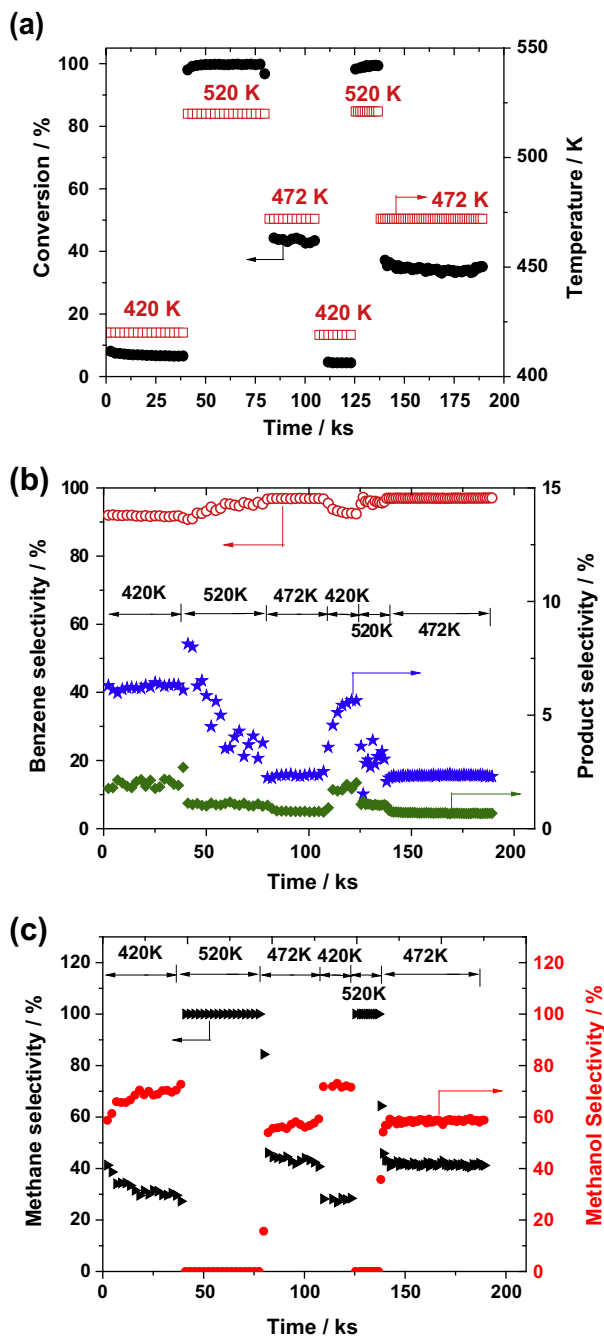


Fig. 4. (a) Conversion of anisole, (b) measured selectivity for benzene (○), cyclohexane (★) and sum of toluene, styrene and phenol (◆) and (c) measured selectivity for methane (▶) and methanol (●) on Mo₂C (sample #8 in Table 1) as a function of temperature and time-on-stream at 1 atm. Reaction conditions: anisole/H₂ = ~0.14%/bal (total flow rate ~1.67 cm³ s⁻¹), space velocity ~17 cm³ s⁻¹ g_{cat}⁻¹ and catalyst loading ~97 mg.

SI), suggesting that C₁ species are formed in hydrogenolysis reactions of the Ar–OCH₃ bond in anisole, rather than dissociation of C₆⁺ products. C₁ species are therefore, not included in the C₆⁺ selectivity calculation.

Low cyclohexane selectivity (<9%; no cyclohexane was observed) showed that vapor-phase anisole HDO on Mo₂C catalysts is hydrogen efficient. The observed lower cyclohexane selectivity at the higher reaction temperatures, however, was not thermodynamically, but kinetically controlled because the calculated approach to equilibrium (η , defined as $[P_{\text{cyclohexane}}]/([P_{\text{benzene}}] \times [P_{\text{H}_2}]^3 \times K_{\text{eq}})$; where K_{eq} is the equilibrium constant for

benzene–cyclohexane interconversion) was found to be much smaller than 1.

Two possible explanations for the observed low selectivity to cyclohexane during vapor-phase anisole HDO reaction are as follows: (i) the coverage of benzene decreases as the reaction temperature increases, resulting in lower probability of the sequential hydrogenation reaction, and (ii) the surface of Mo₂C catalysts is influenced by the presence of oxygen when using an oxygenate as a reactant. Mo₂C catalysts have comparable or even higher turnover rates compared to Ru catalysts for benzene hydrogenation at near ambient temperatures and pressures [34,39,40]. A passivated Mo₂C sample, however, was found to be completely inactive for benzene hydrogenation by Djéga-Mariadassou and coworkers [34]. Fig. 5 shows benzene hydrogenation on Mo₂C catalysts before and after vapor-phase anisole HDO reaction at atmospheric pressure. The cyclohexane specific rate was significantly suppressed in the presence of the anisole, suggesting that the presence of oxygen altered the hydrogenation functionality of the Mo₂C catalysts. Similar suppression in the benzene hydrogenation activity was observed when replacing anisole with methanol or water (Fig. S4, SI). This experimental observation is consistent with the inhibitive relationship between the benzene hydrogenation turnover rate and the residual oxygen content of the Mo₂C catalysts reported by Djéga-Mariadassou and coworkers [34]. We propose that the remarkably high hydrogen efficiency of Mo₂C catalysts in anisole HDO is therefore a consequence of the presence of oxygen-containing species from the reactants, which significantly changes the hydrogenation functionality of Mo₂C catalysts. Along the same lines, different selectivities (decomposition vs. dehydrogenation) have been reported for cyclohexene reactions on C/W(110) pretreated with O₂ at different temperatures, suggesting the possibility of manipulating the catalytic selectivity of transition metal carbides by exposure to oxygen [41].

Methane selectivity increased at the expense of methanol selectivity as the reaction temperature and anisole conversion increased (Fig. 4(c) and Fig. 6), suggesting that the phenolic C–O bond (~422 kJ mole⁻¹) was cleaved first to form methanol and benzene as the primary products and methanol was subsequently hydrodeoxygenated to form methane and water. This contrasts with the high selectivity to phenol and the lack of methanol production during anisole HDO over Co–Mo-based [22,23], transition metal

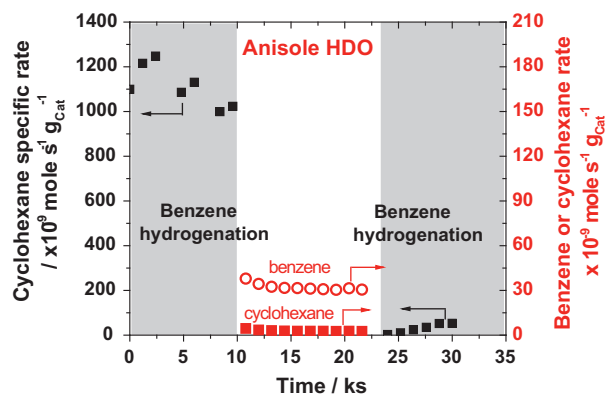


Fig. 5. Cyclohexane production rate measured from either benzene hydrogenation reaction (■, shaded areas) or vapor-phase anisole HDO reaction (■) on a Mo₂C catalyst. Benzene synthesis rate (○) indicates deoxygenation activity. The catalyst was first tested for benzene hydrogenation for ~10 ks (feed composition: benzene/H₂ = 0.23%/bal with total flow rate ~1.67 cm³ s⁻¹) and then switched to vapor-phase anisole HDO reaction (feed composition: anisole/H₂ = 0.14%/bal with total flow rate ~1.67 cm³ s⁻¹), followed by restoring the reaction conditions to benzene hydrogenation. The reaction temperature was maintained at ~423 K under ambient pressure during the switch of aforementioned two different reactions. Catalyst loading was ~150 mg.

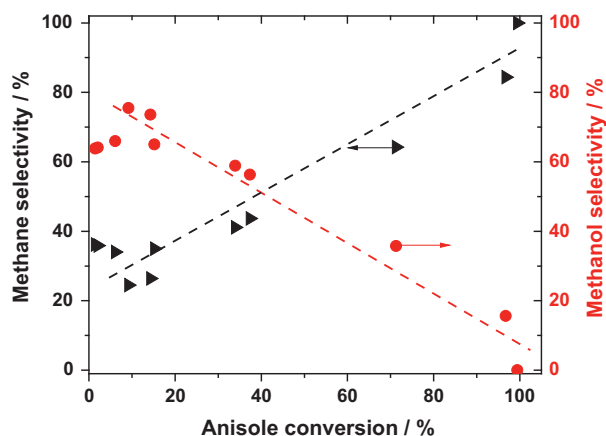


Fig. 6. Selectivity of methane (\blacktriangleright) and methanol (\bullet) as a function of anisole conversion; a range of anisole conversion was achieved by using different amounts of catalyst or varying the reaction temperature. Reaction conditions: anisole/ $H_2 = \sim 0.14\%$ /bal (total flow rate $\sim 1.67 \text{ cm}^3 \text{ s}^{-1}$), and catalyst loading ~ 11 to $\sim 140 \text{ mg}$. The dashed lines are drawn to guide the eyes.

sulfide [17,19], and Pt-based catalysts [21], wherein the weaker aliphatic C–O bond ($\sim 339 \text{ kJ mole}^{-1}$) was preferentially cleaved. The occurrence of demethoxylation, instead of demethylation, for vapor-phase anisole HDO on Mo_2C was further supported by the very low selectivity to phenol, $<1\%$, at all anisole conversions (0.6–100%).

Benzene synthesis rate ($\text{mole s}^{-1} \text{ g}_{\text{cat}}^{-1}$) was independent of anisole chemical conversion (0.6–14%) achieved using different amounts of catalysts (sample #8 in Table 1 and 0.03–0.14 g) as shown in Fig. S6 in the SI. This experimental result shows there is no product inhibition and/or the effects of product concentration gradients on the benzene synthesis rate can be neglected at the current reaction conditions.

Fig. 7(a) shows that the rate of benzene synthesis does not depend on anisole pressure (0.06–1.1 kPa), indicating the surface is predominantly covered by anisole-derived intermediates. The concurrent near half-order (~ 0.6) dependence of benzene synthesis rates on H_2 pressure (Fig. 7(a)) at constant anisole pressure ($\sim 0.14 \text{ kPa}$) suggests that dissociative adsorption of hydrogen occurs, however, on sites that are distinct from those required for anisole adsorption because if competition between anisole and molecular hydrogen existed for the same site, we would observe inhibition of catalytic rates by anisole. The hydrogen order was also found to be independent of the anisole concentration (0.12–0.96 kPa) as shown in Fig. 7(b), confirming that distinct sites are required for hydrogen and anisole activation.

It was suggested by Ko and coworkers that CO can molecularly chemisorb on exposed on-top sites of Mo on a carbided Mo (100) surface, while dissociative H_2 chemisorption can occur across four-fold hollow sites of the carbide surfaces [42]. These surface science studies are consistent with positive reaction orders for both H_2 and CO in CO hydrogenation reactions, suggesting that CO adsorption does not inhibit H_2 chemisorption [43]. Similarly, we postulate anisole adsorption can occur on sites resembling those required for CO chemisorption (CO chemisorption sites are involved in vapor anisole HDO as we discuss in Section 3.3), while another type of site, such as fourfold hollow sites, may be responsible for H_2 activation.

The apparent activation energy was found to be $\sim 76 \pm 1.3 \text{ kJ mole}^{-1}$ (Fig. S7, SI). Fig. 8(a) and (b) show that both the hydrogen order and the apparent activation energy were invariant with anisole conversion (~ 0.6 –15%, achieved by varying catalyst weight over a range of 0.03–0.14 g), which confirms that the products of anisole HDO do not have measurable kinetic effects on the benzene synthesis rate under these reaction conditions.

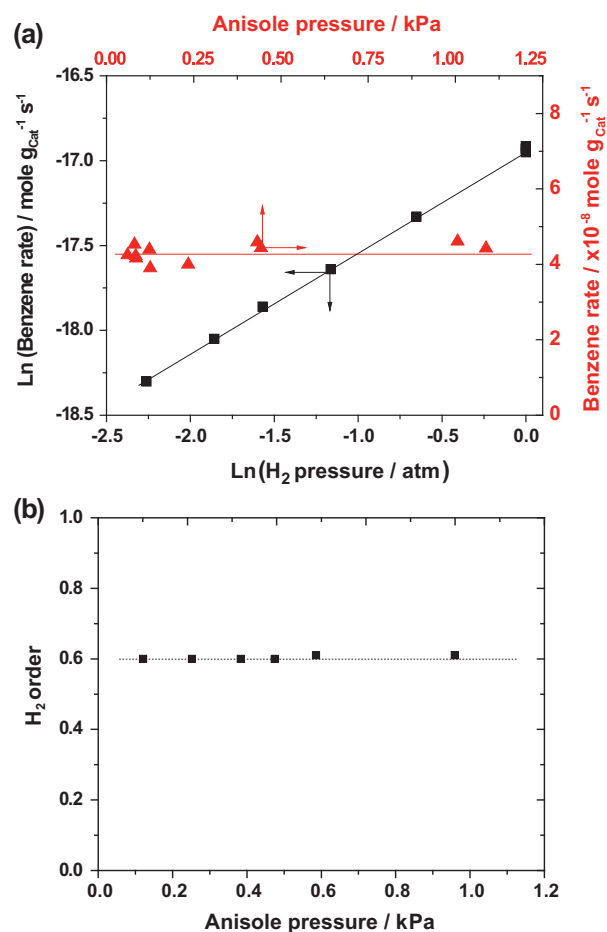
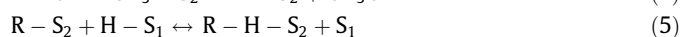
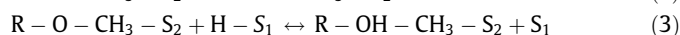
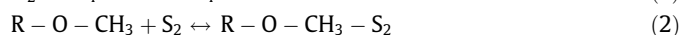


Fig. 7. (a) Effect of H_2 pressure (\blacksquare) varied from ~ 0.1 to $\sim 1 \text{ atm}$ (balance He) at $\sim 0.14 \text{ kPa}$ anisole at 423 K and anisole pressure (\blacktriangle) varied from ~ 0.06 to $\sim 1 \text{ kPa}$, balance H_2 at 423 K and (b) hydrogen order measured at different anisole concentrations. Experimental data obtained at 423 K, total pressure = 1 atm.

A plausible reaction mechanism involving the addition of dissociated hydrogen to adsorbed anisole is proposed to account for the experimentally observed reaction order dependencies: zero order for anisole, $\sim 1/2$ order for hydrogen and no kinetic effects of anisole HDO products on the benzene synthesis rate. Hydrogen molecules undergo dissociative adsorption on site 1 (S_1), while anisole molecules (R represents a C_6H_5 functional group) adsorb on a distinct site 2 (S_2) [Eqs. (1) and (2)]. The dissociated hydrogen first binds to the oxygen atom of the adsorbed anisole to give an anisole-derived intermediate [Eq. (3)] that facilitates the cleavage of the phenolic C–O bond, presumably because of the strong interaction between the carbidic surface [44–46] and the benzene ring, to generate methanol (4), followed by a sequential addition of dissociated hydrogen to form benzene adsorbed on S_2 [Eq. (5)]. The adsorbed benzene can then desorb [Eq. (6)] to complete the catalytic cycle.



Based on the assumption that (1) cleavage of the strong phenolic C–O bond is the rate-determining step [Eq. (4)], (2) all other steps are at quasi-equilibrium, and (3) the most abundant reactive

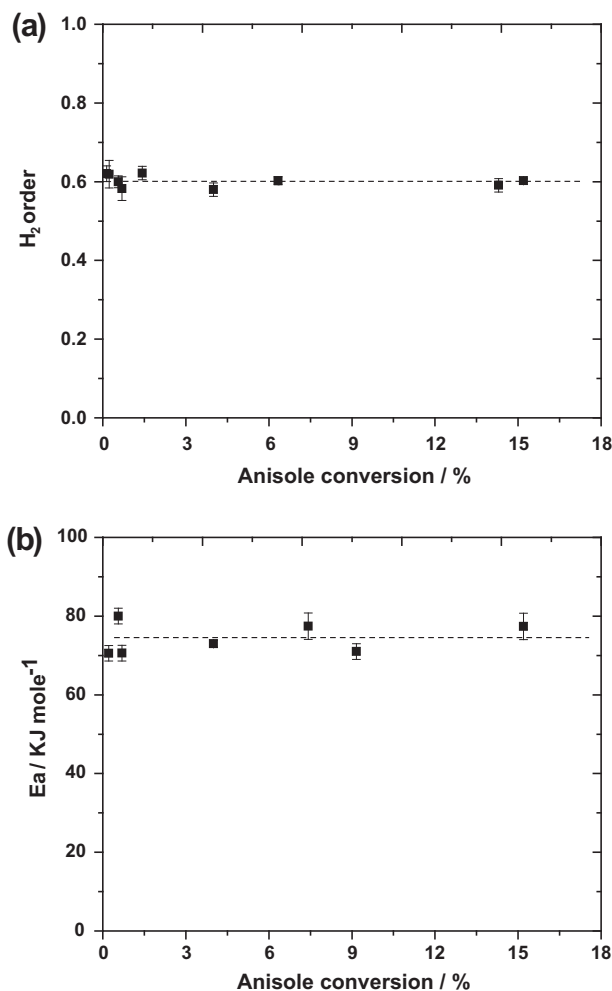
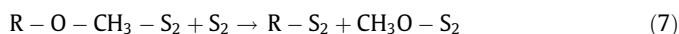


Fig. 8. (a) Hydrogen order and (b) apparent activation energy as a function of anisole conversion. Experimental data obtained at 423 K, H₂ pressure varied from ~0.1 to ~1 atm (balance He) at ~0.14 kPa anisole, total pressure = 1 atm. Anisole conversion was adjusted by using different amounts of Mo₂C catalysts (0.03–0.14 g) with total flow rate ~1.67 cm³ s⁻¹.

intermediate (MARI) for site 2 (S₂) is anisole (R–O–CH₃–S₂) and site 1 (S₁) is predominantly empty, a rate equation for benzene synthesis consistent with the experimentally observed zero-order dependence in anisole and half-order dependence in H₂ can be derived.

Density functional theory (DFT) calculations by Ren et al. have suggested that addition of dissociated hydrogen to an adsorbed propanol molecule on Mo₂C catalysts occurs with an energy barrier exceeding 1 eV, which is similar to the step shown in [Eq. (3)]. If we consider this step [Eq. (3)] to be the rate-determining step, MARI for site 1 (S₁) is empty sites, and the coverage of the adsorbed anisole (R–O–CH₃–S₂) species to be much higher than that for all other adsorbates on S₂ sites, a rate equation for benzene synthesis that can account for experimentally observed zero order in anisole and half order in H₂ can also be derived.

Alternatively, considering that oxygen can bind strongly to the surface of Mo₂C catalysts [28,47,48], the cleavage of the phenolic C–O bond in surface-bound anisole might be facilitated by an adjacent empty site [Eq. (7)], instead of reacting with dissociated hydrogen to form the active intermediate (R–OH–CH₃–S₂, [Eq. (4)]).



Based on the assumptions that (1) the addition of dissociated hydrogen to the benzene ring intermediate adsorbed on S₂ (R–S₂)

is the rate-determining step [Eq. (5)], (2) adsorbed anisole (R–O–CH₃–S₂) and empty sites are the MARI for S₂ and S₁ respectively, the same benzene synthesis rate dependencies with zero order in anisole and ~1/2 order in H₂ can be derived.

The rate equations for benzene synthesis derived from the proposed mechanisms described above can give zero order in anisole and half order in H₂. If we consider that (i) there are two types of sites involved in this reaction, one (S₁) for H₂ dissociation and the other (S₂) for anisole activation [Eqs. (1) and (2)], (ii) a non-uniform surface of S₁ sites and a uniform surface of S₂ sites, and (iii) considering step [Eq. (3)] to be the rate-determining step, the fractional order of 0.6 in H₂ can be derived, as briefly shown below (A detailed derivation can be found in Section 2 in the SI):

We consider [j] such ensembles for the sites S₁ and the concentration of the dissociatively adsorbed hydrogen in ensemble j can be derived from site balance in ensemble j and the equilibrium of [Eq. (1)]:

$$[H-S_1]_j = \left(\frac{k_1}{k_{-1}}\right)^{\frac{1}{2}} \cdot [H_2]^{\frac{1}{2}} \cdot \frac{[L_1]_j}{1 + [H_2]^{\frac{1}{2}} \left(\frac{k_1}{k_{-1}}\right)^{\frac{1}{2}}} \quad (8)$$

The turnover rate, V_{j,t} in each ensemble j for benzene synthesis can be expressed as

$$V_{j,t} = \frac{k_3 k_1^{\frac{1}{2}} \cdot [R-O-CH_3-S_2] \cdot [H_2]^{\frac{1}{2}}}{k_{-1}^{\frac{1}{2}} + k_1^{\frac{1}{2}} [H_2]^{\frac{1}{2}}} \quad (9)$$

According to Boudart and Djega-Mariadassou [49], the rate constants can be related to an equilibrium constant and can be expressed as

$$k_1 = k_1^0 \exp(\alpha(t - t_0)) \quad (10)$$

$$k_3 = k_3^0 \exp((\alpha - 1)(t - t_0)) \quad (11)$$

$$k_{-1} = k_{-1}^0 \exp((\alpha - 1)(t - t_0)) \quad (12)$$

where k₁⁰, k₋₁⁰, and k₃⁰ are rate constants in the limit of full coverage; α is a so-called transfer coefficient, which correlates the forward and reverse rate constant of an elementary step to its equilibrium constant; t is dimensionless affinity defined as positive in the direction of adsorption in which $t = \frac{A^0}{RT}$ and t₀, t₁ represent the upper bound and lower bound respectively.

An average turnover rate, v_t can be obtained by integrating the rates on each ensemble over the entire surface:

$$v_t = \frac{1}{L_1} \int_{t_1}^{t_0} V_{j,t} dL'_j \quad (13)$$

A continuous site distribution is assumed [49] with the form:

$$dL'_j = \frac{[L_1]^\gamma}{\exp(\gamma f) - 1} \exp(-\gamma(t - t_0)) dt \quad (14)$$

where γ is a constant characterizing the site distribution and dL'_j is the concentration of sites with a standard affinity for adsorption of dissociated hydrogen between A⁰ and A⁰ + dA⁰ in the ensemble j and f = t₀ - t₁.

The integrated solution is (the detailed integration procedure can be found in the Section 2 in the SI):

$$v_t = \frac{\gamma}{\exp(\gamma f) - 1} \frac{k_3^0 k_1^{\frac{1}{2}} \cdot [R-O-CH_3-S_2] \cdot [H_2]^{\frac{1}{2}}}{k_{-1}^{\frac{1}{2}}} \frac{2\pi \left[\frac{k_1^{\frac{1}{2}}}{k_{-1}^{\frac{1}{2}} [H_2]^{\frac{1}{2}}} \right]^{2m-1}}{\sin((2m-1)\pi)} \quad (15)$$

where m = α - γ

$$\text{Therefore, } v_t \propto [R-O-CH_3-S_2] \cdot [H_2]^{1-m} \quad (16)$$

The S_2 sites would then be treated with uniform surface kinetics and if we assume the MARI on S_2 is adsorbed anisole species, the order in anisole would be zero and a fractional order of 0.6 for H_2 can be obtained with $m = 0.4$.

3.3. Site requirements of molybdenum carbide catalysts for vapor-phase anisole HDO

The existence of basic, acidic, and metallic catalytic sites on Mo_2C catalysts has been noted in temperature programmed desorption measurements of probe molecules such as NH_3 , CO_2 , and CO , together with probe reaction studies [34,35,50]. The involvement of metallic sites in vapor-phase anisole HDO reaction was demonstrated by the near invariance in the turnover rate (TOR) of catalytic hydrodeoxygenation at 420 K (average value between 1–2 h time-on-stream) normalized by the number of catalytic centers measured by CO chemisorption (ex situ measurement using Micromeritics 2020) at 323 K as shown in Table 2. This is also observed for the sample (#9 in Table 2) prepared by re-carburization of a mixture of multiple batches of Mo_2C catalysts, which reinforces the idea that the number of CO chemisorption sites is a relevant descriptor to assess the number of catalytic centers involved in the vapor-phase HDO of anisole on Mo_2C . Furthermore, the presence of the species that give a diffraction peak at $\sim 26^\circ$ (2θ) has no measurable effects on HDO catalytic rates or benzene selectivity as the normalized benzene synthesis rate (mole s^{-1} mole $_{COsite}^{-1}$) and benzene selectivity for sample #8 (with the XRD peak at ~ 26 (2θ), Fig. 1) and #9 (without the XRD peak ~ 26 (2θ), Fig. S2(b), SI) were almost identical ($\sim 3 \times 10^{-4}$ mole s^{-1} mole $_{COsite}^{-1}$ and $\sim 91\%$, respectively). The near invariance in measured apparent activation energies (~ 70 kJ mole $^{-1}$) and benzene selectivity ($\sim 92\%$) for samples reported in Table 2 suggests that the identity of the active sites and/or the HDO reaction mechanism are similar on all tabulated Mo_2C samples. These experimental results also confirm the absence of heat and mass transfer limitations because the benzene synthesis rate normalized per CO chemisorption site was found to be similar, which satisfies the Koros-Nowak criterion [51].

The existence of multiple active sites on Mo_2C catalysts was further tested by measuring forward rates of H/D exchange and benzene synthesis with and without the presence of a CO co-feed during vapor-phase anisole HDO reactions (Fig. 9). The measured forward rates of H/D exchange and benzene synthesis for Mo_2C catalysts (sample #10 in Table 1) at 406 K in the absence of CO were found to be ~ 3.4 mole $_{HD} s^{-1}$ mole $_{COsite}^{-1}$ and $\sim 8.7 \times 10^{-5}$ mole s^{-1} mole $_{COsite}^{-1}$, respectively. The forward rate of H_2 - D_2 exchange for noble metal based catalysts was reported to be 90–500 mol s^{-1} mole $_{surf}^{-1}$ metal for SiO_2 supported noble metal catalysts by Goel et al. [52]. The much lower forward rates of H/D exchange for Mo_2C catalysts (~ 3.4 mole $_{HD} s^{-1}$ mole $_{COsite}^{-1}$) compared to those for noble metal based catalysts might be attributed to the presence of anisole, an oxygen-containing molecule, which inhibits the surface hydrogenation functionality of Mo_2C formulations as discussed in Section 3.2 and Fig. 5.

Fig. 9 shows that the extent of inhibition by a CO co-feed (~ 0.0125 to 0.125 cm 3 s $^{-1}$) for the forward rates of H/D exchange and benzene synthesis was different. This experimental observation suggests that CO inhibits benzene synthesis, presumably via blocking the sites responsible for anisole adsorption and/or activation, and that H_2 activation likely occurs on a distinct site, since otherwise, the normalized forward rates of H/D exchange would be suppressed to the same extent as the normalized benzene synthesis rates upon the introduction of CO (see Table S3 in the SI for additional information). The inference of the involvement of distinct catalytic sites for the activation of H_2 and oxygen-containing molecules on Mo_2C catalysts from this titration study is consistent

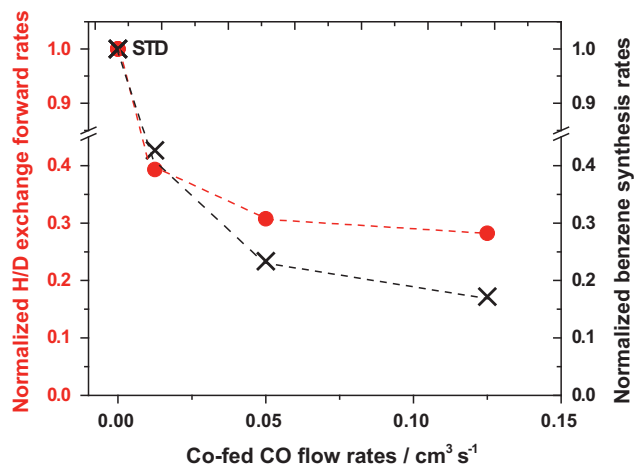


Fig. 9. Effects of CO co-feed during vapor-phase anisole hydrodeoxygenation on normalized benzene synthesis (x) and H/D exchange forward rates (●). Forward rates of H/D exchange and benzene synthesis rates with a CO co-feed (from 0.0125 to 0.125 cm 3 s $^{-1}$) were normalized to those measured under standard conditions (STD, in the absence of CO co-feed) prior to the CO titration. See Table S3 in the SI for measured rates of H/D isotopic exchange and benzene synthesis. CO was co-fed into the reactant mixture comprising anisole/ D_2 / H_2 /Ar (vol%) = $\sim 0.12/40/40$ /bal with a total flow rate ~ 1.67 cm 3 s $^{-1}$ at reaction temperature ~ 406 K under ambient pressure; Mo_2C loading ~ 0.022 g (sample #10 in Table 1). The dashed lines are drawn to guide the eyes.

with kinetics studies and proposed mechanisms discussed in Section 3.2 above to rationalize the measured concurrent zero-order dependence in anisole and near half-order dependence in H_2 observed experimentally.

It is challenging to compare Mo_2C formulations we report with other catalysts used for vapor-phase anisole HDO because (i) the rates reported are typically at varying conversions [15,19,27], (ii) fast catalyst deactivation is encountered in some cases [28], (iii) product inhibition may become relevant for other catalysts, and (iv) the identity of the active sites is not known. Since benzene is not necessarily the dominant product from anisole HDO reactions, the specific rate for deoxygenation products per gram of catalyst and/or the number of active centers assessed by chemical adsorption experiments is compared. Ro \acute{m} an-Leshkov and coworkers reported specific rates for deoxygenation of anisole on MoO_3 catalysts to be $\sim 7.5 \times 10^{-6}$ mole s^{-1} g $_{cat}^{-1}$ with benzene, toluene, xylene and alkylbenzenes as major products at 673 K and 1 atm [27] and that for a 1 wt% Pt/H-BEA bifunctional catalyst to be 3.3×10^{-1} mole s^{-1} mole $_{surface}^{-1}$ Pt with benzene, toluene, xylene and C_5 aromatics as major deoxygenation products at 673 K at 1 atm [15]. Hicks and coworkers reported that $\sim 92\%$ anisole conversion with deoxygenation product selectivity $\sim 96\%$ (90% for benzene and 6% for cyclohexane) could be achieved by a FeMo bimetallic phosphides catalyst (FeMoP) in 0.5 h in a liquid-phase batch reactor, which corresponds to a specific deoxygenation rate of $\sim 1.7 \times 10^{-3}$ mole s^{-1} mole $_{metal}^{-1}$ at 673 K under 4.2 MPa H_2 [19]. The deoxygenation rate based on the rate of benzene synthesis (excluding cyclohexane) for Mo_2C formulations ($\sim 3 \times 10^{-4}$ at 423 K, Table 2) extrapolated to 673 K based on the apparent E_a ~ 70 kJ mole $^{-1}$ (Table 2) and under ambient pressure is $\sim 4.8 \times 10^{-1}$ mole s^{-1} mole $_{COsites}^{-1}$.

Density functional theory (DFT) calculations by Rodriguez and coworkers have suggested that Mo oxycarbide is formed on the surface of a Mo_2C catalyst during water gas shift (WGS) and is responsible for the experimentally observed high WGS activity [47]. The authors proposed that chemisorbed oxygen from water dissociation could be destabilized by the C-terminated Mo_2C (001) surface, which facilitates intermediate strength binding of reaction intermediates and therefore enhances the rate of the

WGS reaction. In this work, since the oxygen in anisole can be removed as either water or methanol, depending on anisole chemical conversion, the possibility of in situ formation of oxycarbide phase during vapor-phase HDO, therefore, cannot be excluded. We also note that the existence or involvement of carbidic or oxycarbide phases [53] cannot be inferred from the CO adsorption studies we report above and the identification of working active phase during HDO reaction requires additional characterization. Although the identity of the two active sites involved in vapor-phase anisole HDO on Mo₂C catalysts cannot be inferred from our results, we report that Mo₂C is a stable and selective catalyst for deoxygenation of aromatic ethers at ambient pressure and low temperatures for the synthesis of aromatics and report kinetic and chemical titration studies to infer the involvement of (i) two distinct sites in this chemistry, and (ii) metallic sites in this chemistry that can be titrated by CO to rigorously calculate catalytic rates.

4. Conclusions

In summary, molybdenum carbide catalysts can convert anisole to benzene in the vapor phase with unprecedented selectivity (>90% among C₆ products), high hydrogen efficiency, (<9% selectivity for the undesired sequential hydrogenation product, cyclohexane) and stable rates at low reaction temperatures (420–520 K) and ambient pressure. The stronger phenolic C–O bond, instead of the weaker aliphatic C–O bond (~422 vs. ~339 kJ mole⁻¹) in anisole was preferentially cleaved during the HDO reaction. The products of anisole HDO showed no measurable kinetic inhibition effects on the benzene synthesis rate. At least two distinct sites are required and metallic sites are involved in vapor-phase anisole HDO on Mo₂C catalysts. The extent of inhibition in benzene synthesis rates was found to be different from that in forward rates of H/D exchange upon co-feeding CO in the reaction mixture, suggesting that the catalytic sites for H₂ activation are distinct from those for anisole adsorption and/or activation. Taken together with the remarkable selectivity for benzene, the relatively low reaction temperature, and low H₂ pressure required to break the phenolic C–O bond, these initial findings show molybdenum carbide is a promising catalyst for catalytic deoxygenation with particular relevance to lignin-derived phenolic ethers.

Acknowledgments

This research was supported by Office of Basic Energy Sciences, the U.S. Department of Energy under award number no. DE-SC0008418 (DOE Early Career Program). Part of this work was carried out in the Characterization Facility of the University of Minnesota, which receives partial support from the National Science Foundation through the MRSEC program. We thank Professor Fabio Ribeiro of Purdue University for helpful technical discussions and Mr. Minje Kang for preparing the Pd/Al₂O₃ catalyst used in this research.

Appendix A. Supplementary material

Supplementary data associated with this article can be found, in the online version, at <http://dx.doi.org/10.1016/j.jcat.2014.07.025>.

References

[1] H.M. Wang, J. Male, Y. Wang, *ACS Catal.* 3 (2013) 1047–1070.

- [2] J. Zakzeski, P.C.A. Bruijninx, A.L. Jongerius, B.M. Weckhuysen, *Chem. Rev.* 110 (2010) 3552–3599.
- [3] G.W. Huber, J.A. Dumesic, *Catal. Today* 111 (2006) 119–132.
- [4] R.W. GosseLink, D.R. Stellwagen, J.H. Bitter, *Angew. Chem. Int. Ed.* 52 (2013) 5089–5092.
- [5] J.Y. He, C. Zhao, J.A. Lercher, *J. Am. Chem. Soc.* 134 (2012) 20768–20775.
- [6] N. Yan, Y.A. Yuan, R. Dykeman, Y.A. Kou, P.J. Dyson, *Angew. Chem. Int. Ed.* 49 (2010) 5549–5553.
- [7] C. Zhao, Y. Kou, A.A. Lemonidou, X.B. Li, J.A. Lercher, *Angew. Chem. Int. Ed.* 48 (2009) 3987–3990.
- [8] D.C. Elliott, *Energy Fuels* 21 (2007) 1792–1815.
- [9] H.Y. Zhao, D. Li, P. Bui, S.T. Oyama, *Appl. Catal. A* 391 (2011) 305–310.
- [10] A. Centeno, E. Laurent, B. Delmon, *J. Catal.* 154 (1995) 288–298.
- [11] B. Donnis, R.G. Egeberg, P. Blom, K.G. Knudsen, *Top. Catal.* 52 (2009) 229–240.
- [12] M.A. Gonzalez-Borja, D.E. Resasco, *Energy Fuels* 25 (2011) 4155–4162.
- [13] D. Meier, J. Berns, O. Faix, U. Balfanz, W. Baldauf, *Biomass Bioenergy* 7 (1994) 99–105.
- [14] J.Q. Bond, D.M. Alonso, D. Wang, R.M. West, J.A. Dumesic, *Science* 327 (2010) 1110–1114.
- [15] X.L. Zhu, L.L. Lobban, R.G. Mallinson, D.E. Resasco, *J. Catal.* 281 (2011) 21–29.
- [16] K.L. Deutsch, B.H. Shanks, *Appl. Catal. A* 447 (2012) 144–150.
- [17] K.L. Li, R.J. Wang, J.X. Chen, *Energy Fuels* 25 (2011) 854–863.
- [18] C.V. Loricera, B. Pawelec, A. Infantes-Molina, M.C. Alvarez-Galvan, R. Huirache-Acuna, R. Nava, J.L.G. Fierro, *Catal. Today* 172 (2011) 103–110.
- [19] D.J. Rensel, S. Rouvimov, M.E. Gin, J.C. Hicks, *J. Catal.* 305 (2013) 256–263.
- [20] R.C. Runnebaum, R.J. Lobo-Lapidus, T. Nimmanwudipong, D.E. Block, B.C. Gates, *Energy Fuels* 25 (2011) 4776–4785.
- [21] R.C. Runnebaum, T. Nimmanwudipong, D.E. Block, B.C. Gates, *Catal. Lett.* 141 (2011) 817–820.
- [22] S.J. Hurff, M.T. Klein, *Ind. Eng. Chem. Fundam.* 22 (1983) 426–430.
- [23] A.L. Jongerius, R. Jastrzebski, P.C.A. Bruijninx, B.M. Weckhuysen, *J. Catal.* 285 (2012) 315–323.
- [24] S.T. Oyama, T. Gott, H.Y. Zhao, Y.K. Lee, *Catal. Today* 143 (2009) 94–107.
- [25] S.T. Oyama, X. Wang, F.G. Requejo, T. Sato, Y. Yoshimura, *J. Catal.* 209 (2002) 1–5.
- [26] Y.Y. Shu, S.T. Oyama, *Chem. Commun.* (2005) 1143–1145.
- [27] T. Prasomsri, T. Nimmanwudipong, Y. Roman-Leshkov, *Energy Environ. Sci.* 6 (2013) 1732–1738.
- [28] H. Ren, W. Yu, M. Saliciccoli, Y. Chen, Y. Huang, K. Xiong, D.G. Vlachos, J.G.G. Chen, *ChemSusChem* 6 (2013) 798–801.
- [29] W.T. Yu, Z.J. Mellinger, M.A. Barteau, J.G.G. Chen, *J. Phys. Chem. C* 116 (2012) 5720–5729.
- [30] J.X. Han, J.Z. Duan, P. Chen, H. Lou, X.M. Zheng, H.P. Hong, *ChemSusChem* 5 (2012) 727–733.
- [31] A.L. Jongerius, R.W. GosseLink, J. Dijkstra, J.H. Bitter, P.C.A. Bruijninx, B.M. Weckhuysen, *ChemCatChem* 5 (2013) 2964–2972.
- [32] J.A. Schaidle, A.C. Lausche, L.T. Thompson, *J. Catal.* 272 (2010) 235–245.
- [33] J. Patt, D.J. Moon, C. Phillips, L.T. Thompson, *Catal. Lett.* 65 (2000) 193–195.
- [34] J.S. Choi, G. Bugli, G. Djega-Mariadassou, *J. Catal.* 193 (2000) 238–247.
- [35] J.S. Lee, S.T. Oyama, M. Boudart, *J. Catal.* 106 (1987) 125–133.
- [36] F.H. Ribeiro, R.A.D. Betta, G.J. Guskey, M. Boudart, *Chem. Mater.* 3 (1991) 805–812.
- [37] G.S. Ranhotra, G.W. Haddix, A.T. Bell, J.A. Reimer, *J. Catal.* 108 (1987) 24–39.
- [38] E.A. Blekkan, P.H. Cuong, M.J. Ledoux, J. Guille, *Ind. Eng. Chem. Res.* 33 (1994) 1657–1664.
- [39] J.S. Lee, M.H. Yeom, K.Y. Park, I.S. Nam, J.S. Chung, Y.G. Kim, S.H. Moon, *J. Catal.* 128 (1991) 126–136.
- [40] C. MarquezAlvarez, J.B. Claridge, A.P.E. York, J. Sloan, M.L.H. Green, *Stud. Surf. Sci. Catal.* (1997) 485–490.
- [41] N. Liu, S.A. Rykov, J.G. Chen, *Surf. Sci.* 487 (2001) 107–117.
- [42] E.I. Ko, R.J. Madix, *Surf. Sci.* 100 (1980) L449–L453.
- [43] G.S. Ranhotra, A.T. Bell, J.A. Reimer, *J. Catal.* 108 (1987) 40–49.
- [44] X.C. Liu, A. Tkalych, B.J. Zhou, A.M. Koster, D.R. Salahub, *J. Phys. Chem. C* 117 (2013) 7069–7080.
- [45] A.S. Rocha, A.B. Rocha, V.T. da Silva, *Appl. Catal. A* 379 (2010) 54–60.
- [46] B.J. Zhou, X.C. Liu, J. Cuervo, D.R. Salahub, *Struct. Chem.* 23 (2012) 1459–1466.
- [47] P. Liu, J.A. Rodriguez, *J. Phys. Chem. B* 110 (2006) 19418–19425.
- [48] A.J. Medford, A. Vojvodic, F. Studt, F. Abild-Pedersen, J.K. Norskov, *J. Catal.* 290 (2012) 108–117.
- [49] M. Boudart, G. Djéga-Mariadassou, *Kinetics of Heterogeneous Catalytic Reactions*, Princeton University Press, Princeton, 1984.
- [50] S.K. Bej, L.T. Thompson, *Appl. Catal. A* 264 (2004) 141–150.
- [51] S. Koso, Y. Nakagawa, K. Tomishige, *J. Catal.* 280 (1967) 221–229.
- [52] S. Goel, Z.J. Wu, S.I. Zones, E. Iglesia, *J. Am. Chem. Soc.* 134 (2012) 17688–17695.
- [53] H.H. Hwu, M.B. Zellner, J.G.G. Chen, *J. Catal.* 229 (2005) 30–44.